# Elastic scattering of pions from $^3$H and $^3$He into the backward hemisphere

S. K. Matthews,* W. J. Briscoe, C. Bennhold, B. L. Berman, R. W. Caress,† K. S. Dhuga, S. N. Dragic, S. S. Kamalov,‡ N. J. Nicholas,§ M. F. Taragin,‖ and L. Tiator¶
*Center for Nuclear Studies, Department of Physics, The George Washington University, Washington, DC 20052*

S. J. Greene
*Los Alamos National Laboratory, Los Alamos, New Mexico 87545*

D. B. Barlow,** B. M. K. Nefkens, C. Pillai,†† and J. W. Price‡‡
*Department of Physics, University of California, Los Angeles, California 90024*

L. D. Isenhower and M. E. Sadler
*Department of Physics, Abilene Christian University, Abilene, Texas 79699*

I. Šlaus and I. Supek
*Rudjer Bošković Institute, Zagreb, Croatia*
(Received 20 May 1994)

We have measured differential cross sections for the elastic scattering of charged pions from $^3$H and $^3$He into the backward hemisphere. Near the peak of the delta resonance, at $T_\pi = 180$ MeV, an angular distribution covering 114° to 168° in the laboratory extends our earlier measurements. At $T_\pi = 142$, 180, 220, and 256 MeV, we have measured an excitation function at angles approaching 170°. The cross sections for the reactions $^3\mathrm{He}(\pi^+,\pi^+)^3\mathrm{He}$, $^3\mathrm{H}(\pi^-,\pi^-)^3\mathrm{H}$ show a rise at back angles which is not seen for $^3\mathrm{He}(\pi^-,\pi^-)^3\mathrm{He}$ and $^3\mathrm{H}(\pi^+,\pi^+)^3\mathrm{H}$. There is a dip in the cross sections near 130° for $T_\pi = 180$ MeV.

PACS number(s): 25.55.Ci, 25.80.Dj, 21.10.Gv, 25.10.+s

## I. INTRODUCTION

Strongly-interacting probes provide complementary information to that from electron-scattering experiments, in which the probe interacts mainly with the proton distributions, and which specifically give no information about the distribution of the spin-paired neutrons of $^3$He. In this work, we continue our study of the nuclear structure of $^3$H and $^3$He using charged pions as probes, which allow direct interaction with both the neutron and proton distributions of these mirror nuclei.

$^3$H exists predominantly as one proton and two spin-paired neutrons, while $^3$He has a single neutron and two spin-paired protons. The four combinations available with these two targets fall naturally into two groups. The $\pi^-$-$^3$H and $\pi^+$-$^3$He systems have isospin $I = \frac{3}{2}$, while the $\pi^+$-$^3$H and $\pi^-$-$^3$He systems are a mixture of $I = \frac{3}{2}$ and $I = \frac{1}{2}$. Charge symmetry in the strong interaction implies that the members of each pair will have equal cross sections at every angle and energy if we correctly account for the Coulomb interaction.

Since there are only three nucleons in each nucleus, the protons and neutrons of $^3$H and $^3$He are uniquely described by whether or not they are members of a spin-pair, whether they are "even" or "odd." We will refer to the matter radii of the nucleons, that is, their rms separation from the center of mass, as even for the protons in $^3$He and the neutrons in $^3$H, and odd for the neutron in $^3$He and the proton in $^3$H. Because of Coulomb repulsion between protons, we expect that the even radius of $^3$He will be larger than that of $^3$H. Furthermore, since the average proton density of $^3$He is thus decreased, its neutron feels less average attraction from its two protons, and the odd radius of $^3$He is larger than that of $^3$H as well [1]. Because of these increased radii, we expect the matter form factor of $^3$He to be smaller than that of $^3$H for a given momentum transfer, which implies a smaller elastic-scattering cross section.

Formally, for a spin-$\frac{1}{2}$ system such as $\pi$ + nucleon, the

*Present address: Physics Department, Catholic University of America, Washington, DC 20064.
†Present address: Burlington Engineering Labs, North Carolina State University, Raleigh, NC 27612.
‡Present address: JINR, Dubna, Russia.
§Present address: Los Alamos Technology Office at Rocky Flats, P.O. Box 4013, Mail Stop T130A, Golden, CO 80401.
‖Present address: Weizmann Institute of Science, Rehovot 76100, Israel.
¶Present address: Institut für Kernphysik, Universität Mainz, D55099 Mainz, Germany.
**Present address: Los Alamos National Laboratory, Los Alamos, NM 87545.
††Present address: Los Alamos National Laboratory, Los Alamos, NM 87545.
‡‡Present address: Dept. of Physics, Rensselaer Polytechnic Institute, Troy, NY 12180-3590.

 

scattering amplitude can be written as a sum of non-spin-flip [$f(\theta)$] and spin-flip [$g(\theta)$] parts, where $\theta$ is the $\pi$ – nucleon center-of-mass scattering angle. Near the peak of the delta resonance, at $T_\pi = 180$ MeV, the angular dependence of the non-spin-flip and spin-flip $\pi$ – nucleon amplitudes is that of the cosine and sine, respectively, of the scattering angle. In the specific case of scattering charged pions from bare nucleons near the delta-resonance energy, conservation of total isospin and neglect of the $I = \frac{1}{2}$ amplitude compared to the $I = \frac{3}{2}$ amplitude leads to the correct prediction that the cross sections for the I $= \frac{3}{2}$ interactions $\pi^+p$ and $\pi^-n$ will be approximately nine times as large as the cross sections for the mixed-isospin interactions $\pi^-p$ and $\pi^+n$. Thus at this energy we expect that single scattering from a nucleus will be dominated by the $\pi^+p$ and $\pi^-n$ interactions; we will refer to the $\pi^+$-$^3$He and $\pi^-$-$^3$H interactions as "even-nucleon" interactions and the $\pi^+$-$^3$H and $\pi^-$-$^3$He interactions as "odd-nucleon" interactions.

Now consider the odd-nucleon interactions, $\pi^-$-$^3$He, for example. The largest amplitude is for $\pi^-n$ scattering from the unpaired neutron. At 90° in the $\pi$ – nucleon center of mass, the non-spin-flip amplitude has a minimum, which is filled in by spin-flip scattering from the neutron. In the even-nucleon case, $\pi^+$-$^3$He, the largest amplitude is $\pi^+p$ scattering from the paired protons. In this case, the spin-flip interaction with either proton is forbidden by the Pauli principle, and so the dip is not filled in. We call this dip in the even-nucleon cross sections, which occurs at about 78° in the laboratory, the non-spin-flip dip (NSF dip).

Forward-angle elastic-scattering data at the delta-resonance energy can be represented very well by a simple, static-nucleon, single-scattering impulse calculation [2]. As the scattering angle approaches 90° in the $\pi$ – nucleon center of mass, it becomes kinematically impossible to reach the $\pi$ – nucleus momentum transfer by scattering from a single, static nucleon [2]. Therefore, scattering from nucleons with nonzero Fermi momentum, as well as second-order effects, become more important. Unfortunately, this limit is reached just forward of the angle corresponding to the NSF dip.

In the experiments reported here, we have scattered pions from $^3$H and $^3$He into the backward hemisphere. We have measured the angular distribution for elastic scattering of 180-MeV pions from 114° to 168° in the laboratory. This distribution is a continuation of our earlier experiments [2–5] which covered the range 40° to 110°. At 142-, 180-, 220-, and 256-MeV incident-pion energy, we have measured an excitation function near 170°. Forward-hemisphere data were obtained in the earlier experiments at 142 MeV and some data were obtained earlier at 220, 256, and 295 MeV in the NSF dip region.

## II. EXPERIMENT

### A. Experimental setup

The experiments were done using the energetic pion channel and spectrometer (EPICS) at LAMPF. The channel produces a momentum-dispersed beam ($dp/p = \pm 1\%$) with a rectangular cross section, 20 cm in the momentum-dispersion (vertical) direction by 8 cm wide. The EPICS system enables one to reconstruct particle trajectories as well as missing mass, so that correlation of the background with specific target regions is possible.

For these backward-angle experiments, we added the EURYDICE dipole magnet at the pivot point of the spectrometer [7], and placed the target at the magnet's center, so that both incoming and outgoing particles were bent through approximately 30°. With this system, we could measure the scattering of 180 MeV pions as far back in angle as 170° in the laboratory.

Three targets at a time could be kept inside the scattering chamber and moved in and out of the beam by means of a turntable target changer. We verified that the contribution to the background of the two targets that were not at the chamber's center was negligible.

Ray tracing showed that the combination of using the bending magnet with targets that have substantial thickness in the direction parallel to the beam (and to the scattered pions) increases the spectrometer acceptance to approximately ±5° full width at half maximum. Thus, each cross section reported here is effectively averaged over this angular width. Due to differences in magnetic field and target-particle mass, the size of this effect was slightly different for $^3$H and $^2$H elastic scattering; we have corrected the cross sections by 1–2 % to account for this difference.

### B. Targets

The targets were aluminum canisters developed expressly for this type of ratio experiment in a joint LAMPF-UCLA project. They were upright cylinders with a wall thickness of 0.18 cm with thick stainless steel end caps bolted to flanges at each end (see [3] for a detailed description of the targets). The $^3$H canister held 18 gm (approximately 180 000 Ci) of $^3$H.

We measured both $\pi^+$ and $\pi^-$ elastic-scattering yields for $^3$H and $^3$He as well as for $^2$H, the latter for normalization to the published $^2$H cross sections of Ottermann *et al.* [6]. We determined target densities by weighing the filled targets, whose volume was known to better than 0.05%. We estimate that expansion and compression of the volume due to variations in temperature and pressure are less than 0.05% as well.

We weighed each target several times, both empty and full, correcting the weights for air buoyancy, derived from temperature and pressure measurements at the time of the weighings. We estimate the uncertainty in the weights at less than 0.6%, mostly due to the buoyancy corrections.

Because the weights always appear in ratios [e.g., $weight(^2\mathrm{H})/weight(^3\mathrm{H})$ in the expression for the $^3$H cross section], the systematic uncertainty due to weighing is $(0.6\% + 0.05\% + 0.05\%)/\sqrt{2} = 0.5\%$. As the weighings were done over many months for the different targets, and repeated in some cases and not in others, and so are essentially random, we have simply added this 0.5%

in quadrature into the statistical uncertainties associated with each cross section; at any rate, in most cases this systematic uncertainty is negligible compared to statistical and systematic uncertainties discussed below.

The purity of the target gases was determined in previous experiments to be better than 99.9% for all targets except $^3$H, which was refilled for this experiment. Previous $^3$H samples from the same source were measured to be better than 99.9% pure as well, but measurement of the sample used for this experiment was not possible, and it was therefore *assumed* to be 100% pure on the day it was filled; yields were corrected for decay from that date. If we assume a 0.1% systematic uncertainty due to impurities in each target, and recalling that each cross section will be calculated as a ratio of target gas and normalization-target gas, we find a maximum 0.14% uncertainty in the ratio (two 0.1% uncertainties added in quadrature). This possible systematic uncertainty is *not* included in the quoted uncertainties.

### C. Background subtraction

We determined the yields from histograms of the missing mass. Typically, the $\pi$-$^3$H and $\pi$-$^3$He elastic peaks were well resolved, and the background under them could be represented by a straight line. This was verified by pion scattering from the $^2$H target with the spectrometer tuned for $\pi$-$^3$H kinematics. $^2$H was used to estimate the background instead of an empty target in order to get a better representation of multiple scattering and energy loss. In Fig. 1 we show the application of this technique to a typical spectrum. The yield is calculated from the number of counts in the peak above the line and inside the points where a smooth curve drawn through the data would cross the line.

Using straight lines to approximate the background greatly decreased the systematic uncertainties in various cross-section ratios which we will report in a later paper. We estimate that systematic uncertainties due to mispositioning of this background line are on the order of 2–3 % for the $^3$H and $^3$He data, and as high as 8% for some of the $^2$H normalization data, because of the difficulty in identifying the counts due to breakup of $^2$H, which occurs at only 2.225-MeV excitation, and thus overlaps the $\pi$-$^2$H elastic-scattering peak.

As was mentioned above, we have extracted these yields by drawing straight lines under the peaks, using the background to either side of the peaks as a guide. In order to assign a statistical uncertainty to the yields, we consider two cases.

First, if we had been able to measure the background shape very accurately, for example by a very long run with a background target such as $^2$H, then there would be negligible uncertainty due to the background. In this case, the statistical uncertainty would be just the square root of the number of counts under the peak, $\sqrt{A+B}$, where $A$ and $B$ are the number of counts in the spectrum, under the peak, above and below the background line, respectively (see Fig. 1).

The second case is that we measure the background line with the same statistics as we measure the peak, and subtract the background counts from the foreground counts. The uncertainty in this case is the standard result, $\sqrt{A+2B}$, which assumes no knowledge of the background shape.

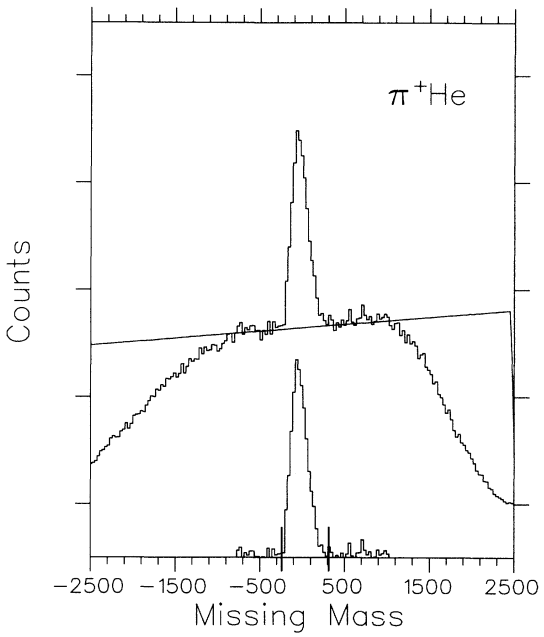


FIG. 1. An example of a spectrum analyzed by drawing a straight line through the background to either side of the elastic peak; in this case, the interaction is $\pi^+$ $^3$He at a laboratory scattering angle of 155°. The spectrum and line, which is drawn by an interactive program that allows the user to specify two points, is shown above the peak that is left after subtracting the counts under the line. The dark bars show the assumed width of the peak.

In our case, the uncertainty is somewhere between these two extremes, as we have used the information of the background shape to the sides of the peak, but not over a very wide part of the spectrum. As a compromise between the two cases, we have used $\sqrt{A+\frac{3}{2}B}$ as the statistical uncertainties of the yields.

### D. Normalization cross sections

It was necessary to interpolate in both angle and energy to match the kinematics of the normalization data to our experimental points. Additionally, we have used the extrapolated 180° points from Ottermann *et al.* [6] for interpolation in those cases where our data were obtained at angles larger than the largest normalization-data angle. Thus uncertainties in the normalization cross sections come from three sources: the statistical and systematic uncertainties quoted by Ottermann *et al.* (each on the order of 4–5 % for the different points), and an interpolation uncertainty estimated by us for each point. The latter varies from less than 1% for the 180-MeV points, to 8% for the 142-MeV points. Table I shows the interpolated laboratory-cross-section values used for our

TABLE I. Differential $\pi^+$-$^2$H cross-section interpolations, in the laboratory frame, in mb/sr. First parenthesis, statistical uncertainties. Second parenthesis, 5% systematic uncertainties added linearly to systematic interpolation uncertainties.

| $\theta_{c.m.}$(deg) | $d\sigma/d\Omega$ (mb/sr) |
|---|---|
| $T_\pi$(lab) = 142 MeV | |
| 158.0 | 1.07 (0.06) (0.12) |
| 162.0 | 1.07 (0.06) (0.12) |
| $T_\pi$(lab) = 180 MeV | |
| 114.0 | 0.52 (0.03) (0.03) |
| 125.0 | 0.46 (0.03) (0.03) |
| 135.0 | 0.40 (0.02) (0.02) |
| 145.0 | 0.39 (0.02) (0.02) |
| 155.0 | 0.37 (0.02) (0.02) |
| 168.0 | 0.39 (0.02) (0.02) |
| $T_\pi$(lab) = 220 MeV | |
| 168.0 | 0.17 (0.01) (0.01) |
| $T_\pi$(lab) = 256 MeV | |
| 168.0 | 0.12 (0.01) (0.01) |

normalizations. Also shown are the interpolated statistical uncertainties, and a systematic uncertainty for each point that was calculated by adding linearly the cited maximum systematic uncertainty of 5% and our own estimate of the systematic uncertainty in the interpolation process, calculated for each point and based on the slope of the normalization cross section in the area of each data point.

### E. Charge asymmetry in $\pi^\pm$ $^2$H

For this analysis we have assumed that the elastic-scattering cross sections for the $\pi^+$-$^2$H and $\pi^-$-$^2$H reactions were equal, and, as mentioned above, we have used the $\pi^+$-$^2$H data of Ottermann *et al.* [6] to normalize our yields. However, Smith *et al.* have measured an asymmetry of 1.5% in these $\pi$-$^2$H reactions in the backward hemisphere [8]. To include this result in our analysis, we would *decrease* the $\pi^-$ cross sections by 3%. We have not included this systematic variation in the tables or graphs.

## III. RESULTS

The results of the experiments are summarized in Table II. The 180-MeV cross sections are shown in Fig. 2. The filled diamonds represent the data from this experiment. At forward angles, the NSF dip is clearly visible

TABLE II. Differential cross sections for the elastic scattering of pions from $^3$H and $^3$He, in the center of mass frame, in mb/sr. First parenthesis, statistical uncertainties from experimental yields and normalization data, added in quadrature. Second parenthesis, systematic uncertainties from this experiment only. The worst-case systematic uncertainty is derived by *adding* linearly the terms in the second parenthesis in each table. As is discussed in the text, the angular acceptance was about ±5° FWHM.

| $\theta_{c.m.}$(deg) | $\pi^+$-$^3$H | $\pi^+$-$^3$He | $\pi^-$-$^3$H | $\pi^-$-$^3$He |
|---|---|---|---|---|
| | | $T_\pi$(lab) = 142 MeV | | |
| 160.0 | 0.91 (0.06) (0.06) | 1.20 (0.07) (0.07) | 1.11 (0.08) (0.07) | 0.82 (0.06) (0.05) |
| 163.6 | 0.86 (0.05) (0.05) | 1.27 (0.07) (0.08) | 1.07 (0.00) (0.06) | 0.76 (0.06) (0.05) |
| | | $T_\pi$(lab) = 180 MeV | | |
| 119.4 | 0.40 (0.02) (0.02) | 0.47 (0.03) (0.03) | 0.47 (0.03) (0.03) | 0.38 (0.02) (0.02) |
| 129.8 | 0.32 (0.02) (0.02) | 0.36 (0.02) (0.02) | 0.38 (0.03) (0.02) | 0.28 (0.02) (0.02) |
| 139.1 | 0.27 (0.02) (0.02) | 0.36 (0.02) (0.03) | 0.37 (0.03) (0.03) | 0.24 (0.02) (0.02) |
| 148.3 | 0.27 (0.02) (0.04) | 0.49 (0.04) (0.06) | 0.48 (0.04) (0.06) | 0.23 (0.02) (0.03) |
| 157.4 | 0.28 (0.02) (0.02) | 0.62 (0.05) (0.04) | 0.64 (0.05) (0.04) | 0.24 (0.02) (0.02) |
| 169.2 | 0.29 (0.02) (0.02) | 0.76 (0.05) (0.06) | 0.72 (0.05) (0.06) | 0.24 (0.02) (0.02) |
| | | $T_\pi$(lab) = 220 MeV | | |
| 169.3 | 0.13 (0.01) (0.01) | 0.31 (0.02) (0.04) | 0.30 (0.02) (0.04) | 0.10 (0.01) (0.01) |
| | | $T_\pi$(lab) = 256 MeV | | |
| 169.4 | 0.052 (0.005) (0.004) | 0.11 (0.01) (0.01) | 0.11 (0.01) (0.01) | 0.041 (0.003) (0.007) |

near 70° in the even-nucleon cases, namely $\pi^-$-$^3$H and $\pi^+$-$^3$He. It has been largely filled in by spin-flip scattering from the odd nucleon for $\pi^+$-$^3$H and $\pi^-$-$^3$He. A second dip is visible in the even-nucleon ($\pi^+$-$^3$He and $\pi^-$-$^3$H) cross-section plots, near a laboratory angle of 130°. This dip can also be seen in the odd-nucleon cross-section plots, although not as clearly. Beginning at about 140° in the laboratory, there is a sizable rise in the even-nucleon cross sections, but not in the odd-nucleon ones.

Figure 3 shows the largest-angle points at each of the energies, 142, 180, 220 and 256 MeV, as a function of the momentum transfer squared; the 180-MeV point is the same as the largest-angle point shown in the angular distribution in Fig. 2. The similarity of the elastic cross sections for $\pi^+$-$^3$H and $\pi^-$-$^3$He, and for $\pi^-$-$^3$H and $\pi^+$-$^3$He, is evident here as well. As in the 180-MeV case, the even-nucleon cross sections are larger than the odd-nucleon ones.

### Back-angle dip

In addition to the NSF dip at approximately 78° in the laboratory, for incident 180-MeV pions, another dip can be seen in the $\pi^+$-$^3$He and $\pi^-$-$^3$H cross sections, near a laboratory scattering angle of 130°, or, a momentum transfer of approximately 5.8 fm$^{-2}$. This same dip is visible in the $\pi^-$-$^3$He and $\pi^+$-$^3$H cross sections, but the lack of the large-angle rise for these latter two makes the dip less obvious. As discussed earlier, the approximately ± 5° acceptance of the spectrometer at these kinematics means that the dip may be filled in somewhat in our data, and might actually be much deeper and narrower than it appears here.

This second dip can be seen in the $\pi$-$^4$He elastic cross-section data as well [9–11]. We have extracted the value of the square of the momentum transfer corresponding to each dip from the cited papers, and plotted them in Fig. 4 (filled circles) as a function of incident pion energy. Values for the $\pi$-$^3$He reaction, from [12], at 295 MeV (the two open squares show the momentum transfer for the dip in the $\pi^+$-$^3$He and $\pi^-$-$^3$He cases, which nearly overlap), and from this experiment at 180 MeV (open circle) are also shown. The error bars are ±2.5 fm$^{-2}$, the approximate width of the dip in our data. We have used the same error bars for the dip locations taken from the other papers, although, especially at the higher energies

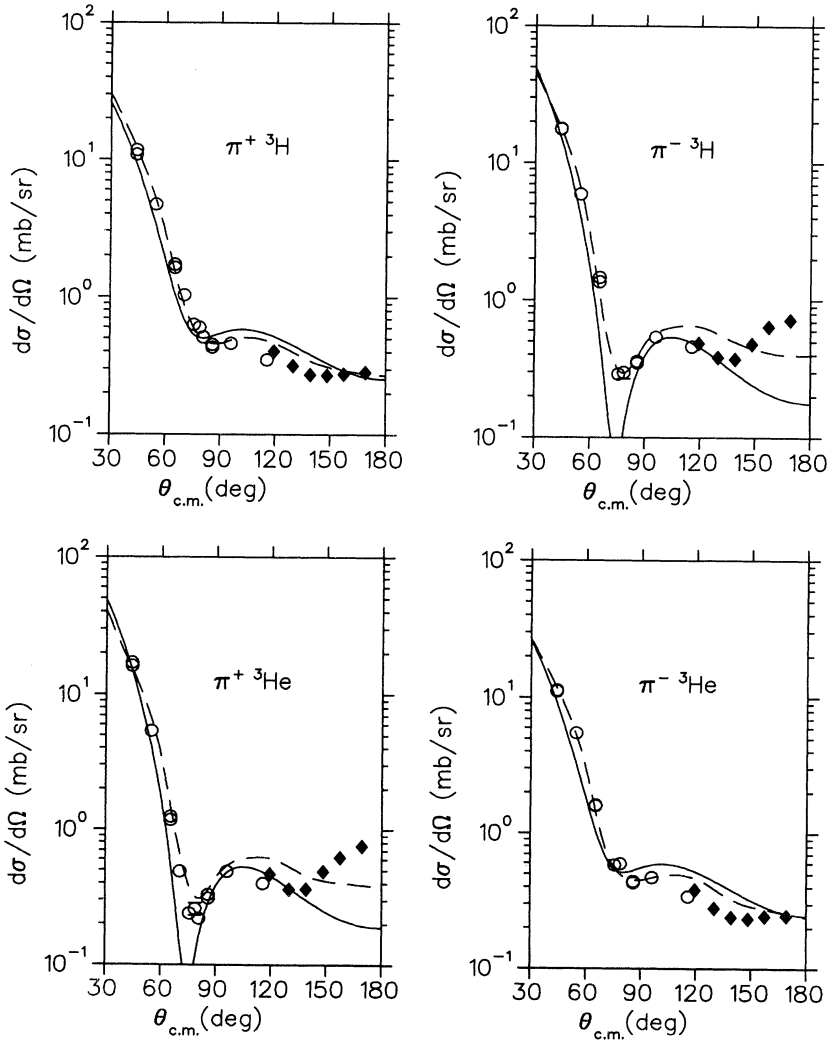


FIG. 2. Cross sections at 180 MeV, compared with recent calculations; the filled diamonds represent the new data. Note the deviation of the calculated results from the "even-nucleon" scattering ($\pi^-$-$^3$H and $\pi^+$-$^3$He) data at large angles. Dashed line: Gibbs and Gibson; solid line: KTB second-order calculation.

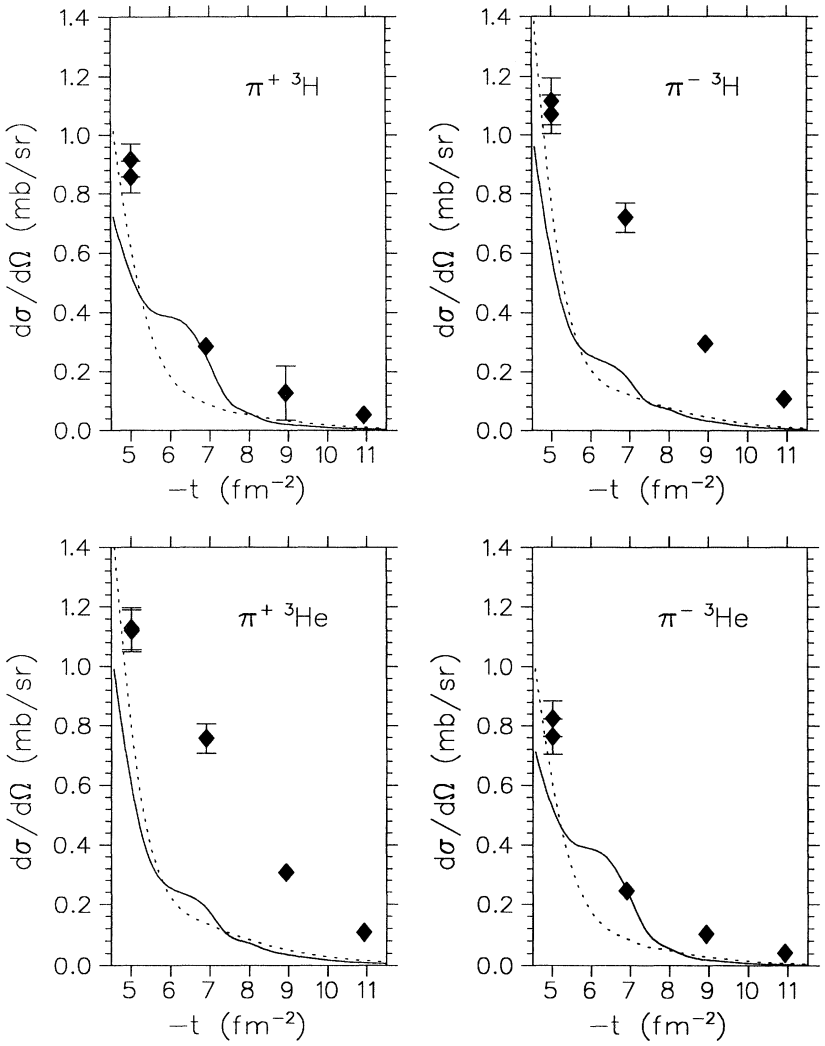


FIG. 3. Largest-angle cross sections for each incident energy (see Table II), plotted as a function of the square of the momentum transfer at that energy and angle, compared with calculated values from KTB. Dotted line: first-order optical potential; solid line: second-order potential.

in these papers, the location is less precise. The $^3$He and $^4$He dip locations increase monotonically with energy over this region.

Charge form factors extracted from electron scattering on $^3$H and $^3$He, which were used in the simple calculation referenced earlier [2], have their first minimum at a momentum transfer of nearly 11 fm$^{-2}$, after correction for the charge form factor of the proton. These corrected form factors, or "matter" form factors, should represent the spatial distribution of the nucleons in the nucleus. As the incident-pion energy approaches 180 MeV, one sees from our data, and from the $^4$He data as well, that the dip in the backward hemisphere occurs for a much lower momentum transfer; in the simple model, with form factors of the form $\exp(-tR^2)$, where $R$ is the rms radius of the nucleon in the nucleus, this would mean an increase in $R$ of about 40%. One would predict a decrease in $R$ and thus an increase in the momentum-transfer corresponding to the dip as the incident pion energy continues to decrease below the delta-resonance energy. However, this momentum transfer is not accessible at lower incident-pion energies, so confirmation is not possible.

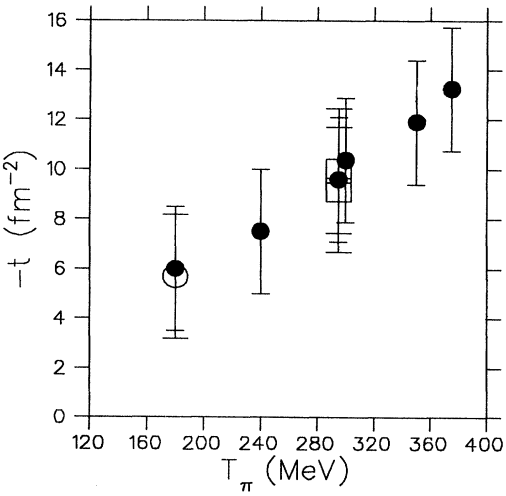


FIG. 4. Momentum transfer of the backward-hemisphere dip locations for $^4$He (filled circles) and $^3$He (open squares, dips for $\pi^-$-$^3$He and $\pi^+$-$^3$He), and for our data (open circle), as a function of the energy of the incident pions.

In analyzing data for pion scattering from heavier nuclei (see, for example, [13] and references cited therein), several prescriptions for improving the fit of optical-model calculations over the entire angular range were found to vary the predicted location of the dip, as well as other features of the differential cross sections. These prescriptions include (1) varying the rms radius of the nucleons in the nucleus, (2) varying the effective interaction energy in the $\pi -$ nucleon $t$ matrix, and (3) adding phenomenological terms dependent on the square of the nucleon density to the optical potential.

We note that the trend shown in Fig. 4 is that the location of the dip in momentum transfer decreases as the incoming pion energy approaches 180 MeV. If we think of the "size" of the nucleon increasing as the resonance energy is approached, then the increased size of the nucleons on the surface of the nucleus would lead to an increased radius of the "disk" presented to the incident pion by the nucleus.

## IV. CALCULATIONS

In this section, we compare the measured cross sections with the results of two different calculations which treat pion-nucleus scattering in the framework of multiple-scattering theory.

In a recent paper by Kamalov, Tiator, and Bennhold (KTB) [14], the $\pi^{\pm}$ -trinucleon scattering matrix $T(E)$ is given as a solution of the Lippmann-Schwinger equation

$$T(E) = V(E) + V(E)G(E)T(E),$$

where $G(E)$ is the pion-nucleus Green's function. This equation is solved in momentum space and therefore treats nonlocalities exactly. The matrix elements are evaluated using realistic correlated three-body wave functions by solving the Faddeev equations using the Reid potential as the $NN$ interaction. The optical potential $V(E) = V_1(E) + V_2(E)$ contains a first-order term $V_1(E)$ and a phenomenological term $V_2(E)$ which represents true pion absorption and higher-order processes. The first-order contribution $V_1(E)$ is related to the free $\pi -$ nucleon $t$ matrix including its full spin and isospin dependence. The second-order term $V_2(E)$ was originally developed for heavier nuclei via the scalar $\rho^2$ term and presently does not include spin and isospin dependence.

These calculations have provided an excellent description of available cross-section and asymmetry data for elastic pion scattering in the energy range $T_\pi = 50 - 300$ MeV [14]. The results of this calculation are shown in Fig. 2 (solid line). In all four cases, the angular distribution is well predicted up to about 110°, which is the limit of the older data. In the backward hemisphere, the calculation does a good job for the odd-nucleon cases, $\pi^+$-$^3$H and $\pi^-$-$^3$He, but does not reproduce the sharp upswing for the even-nucleon cases, $\pi^-$-$^3$H and $\pi^+$-$^3$He.

The other calculation shown (dashed line), by Gibbs and Gibson [1], was done to study the forward-angle data. We note, however, that their back-angle results are similar to the KTB calculation and somewhat closer to the data: the odd-nucleon scattering is well reproduced, but the even-nucleon scattering is not.

Figure 3 shows results of the KTB calculation for the angles near 180°. Once again, the discrepancy between the even- and odd-nucleon scattering is obvious. At 180 MeV, the second-order calculation has a bump and goes through the data in the odd-nucleon cases. For even larger momentum transfer, none of the data points is reproduced by the theory.

Let us briefly consider the shortcomings of the present (KTB) calculations. They are performed in the so-called coherent approximation, which allows only three-nucleon ground states as intermediate states in the multiple-scattering series. However, this excludes certain classes of double-scattering processes, such as sequential spin-flip scattering from paired nucleons.

Another shortcoming of presently available calculations is the inadequate description of two-body terms. The results obtained with the KTB second-order potential should be regarded as very preliminary, since no spin and isospin dependence was included in the $V_2$ term. In the calculations shown in Figs. 2 and 3, the $V_2$ term is of isoscalar, non-spin-flip nature, and has been extrapolated from heavier nuclei. However, analysis of the single-charge-exchange process at higher energies indicates [14] that the isovector second-order potential may play an important role. In fact, writing the full second-order term as

$$V_2(E) = V_2^{T=0}(E) + V_2^{T=1}(E)\mathbf{t}\cdot\boldsymbol{\tau},$$

where $\mathbf{t}$ and $\boldsymbol{\tau}$ refer to the pion and trinucleon isospin operators, respectively, one obtains $V_2 = V_2^{T=0} + V_2^{T=1}$ for the even-nucleon cases and $V_2 = V_2^{T=0} - V_2^{T=1}$ for the odd-nucleon case. Should the isoscalar ($V_2^{T=0}$) and isovector ($V_2^{T=1}$) components be of equal magnitude, one would obtain an enhancement for the even-nucleon, but a partial cancellation for the odd-nucleon, cases. Qualitatively, this effect is observed in the data.

## V. CONCLUSION

Elastic-scattering cross sections for pions of energy 180 MeV from $^3$H and $^3$He have a dip near 130° in the laboratory. This dip is consistent with dips seen in scattering from $^4$He and from $^3$He at energies in the 180–380-MeV range, where the square of the momentum transfer of the dip increases monotonically with the incident pion energy. At 180 MeV, for angles larger than 140°, there is a significant rise in the cross sections for the $\pi^+$-$^3$He and $\pi^-$-$^3$H cases as compared with the $\pi^+$-$^3$H and $\pi^-$-$^3$He cases. This rise is not predicted by modern optical-model calculations, and thus merits further theoretical consideration.

## ACKNOWLEDGMENTS

We would like to acknowledge many helpful discussions with Dr. C. W. Werntz, Dr. E. H. Harper, Dr. W. R. Gibbs, and Dr. B. F. Gibson. We are grateful to Dr. H. R. Maltrud and to L. Sturgess for extensive work filling and weighing the targets and to E. Matthews for design and construction of the target changer. This work has been supported by NSF Grants No. PHY-8907284 and No. PHY-9122139 and DOE Grants No. DE-FG05-86-ER40270 and No. DE-FG05-86-ER40285.

[1] W. R. Gibbs and B. F. Gibson, Phys. Rev. C **43**, 1012 (1991).

[2] B. M. K. Nefkens, W. J. Briscoe, A. D. Eichon, D. H. Fitzgerald, A. Mokhtari, J. A. Wightman, and M. E. Sadler, Phys. Rev. C **41**, 2770 (1990).

[3] C. Pillai, D. B. Barlow, B. L. Berman, W. J. Briscoe, A. Mokhtari, B. M. K. Nefkens, and M. E. Sadler, Phys. Rev. C **43**, 1838 (1991).

[4] K. S. Dhuga, D. B. Barlow, R. S. Kessler, B. M. K. Nefkens, C. Pillai, J. W. Price, B. L. Berman, W. J. Briscoe, S. K. Matthews, and S. J. Greene, Phys. Rev. C (to be submitted).

[5] B. L. Berman, W. J. Briscoe, K. S. Dhuga, D. A. Hanson, S. K. Matthews, A. Mokhtari, C. S. Smith, D. B. Barlow, B. M. K. Nefkens, C. Pillai, J. W. Price, S. J. Greene, and I. Šlaus, in *Pions in Nuclei*, Proceedings of the International Workshop, edited by E. Oset, M. J. Vicente Vacas, and C. Garcia Recio (World Scientific, Singapore, 1992), p. 161.

[6] C. R. Ottermann, E. T. Boschitz, W. Gyles, W. List, R. Tacik, R. R. Johnson, G. R. Smith, and E. L. Mathie, Phys. Rev. C **32**, 928 (1985).

[7] G. R. Burleson, W. B. Cottingame, K. S. Dhuga, J. A. Faucett, C. P. Fontenla, J. F. Amann, R. L. Boudrie, S. J. Greene, C. L. Morris, N. Tanaka, Z. F. Wang, D. Yusnukis, M. Brown, R. R. Kiziah, E. C. Milner, C. F. Moore, S. Mordechai, D. Oakley, P. A. Seidl, C. L. Blilie, D. Dehnhard, S. Nanda, S. J. Seestrom-Morris, J. D. Zumbro, and K. Maeda, Nucl. Instrum. Methods A **247**, 327 (1986).

[8] G. R. Smith, D. R. Gill, D. Ottwell, G. D. Wait, P. Walden, R. R. Johnson, R. Olszewski, R. Rui, M. E. Sevior, R. P. Trelle, J. Brack, J. J. Kraushaar, R. A. Ristinen, H. Chase, E. L. Mathie, V. Pafilis, R. B. Shubank, N. R. Stevenson, A. Rinat, and Y. Alexander, Phys. Rev. C **38**, 240 (1988).

[9] B. Brinkmöller, C. L. Blilie, D. Denhard, M. K. Jones, G. M. Martinez, S. K. Nanda, S. M. Sterbenz, Yi-Fen Yen, L. G. Atencio, S. J. Greene, C. L. Morris, S. J. Seestrom, G. R. Burleson, K. S. Dhuga, J. A. Faucett, R. W. Garnett, K. Maeda, C. Fred Moore, S. Mordechai, A. Williams, S. H. Yoo, and L. C. Bland, Phys. Rev. C **44**, 2031 (1991).

[10] J. Boswell, G. S. Das, P.C. Gugelot, J. Källne, J. McCarthy, L. Orphanos, R. C. Minehart, R. R. Whitney, and P. A. M. Gram, Nucl. Phys. A **466**, 458 (1987).

[11] J. Källne, J. F. Davis, J. S. McCarthy, R. C. Minehart, R. R. Whitney, R. L. Boudrie, J. McClelland, and A. Stetz, Phys. Rev. Lett. **45**, 517 (1980).

[12] J. Källne, J. F. Davis, J. S. McCarthy, R. C. Minehart, R. R. Whitney, R. L. Boudrie, J. McClelland, and A. Stetz, Phys. Lett. **103B**, 13 (1981).

[13] K. S. Dhuga, G. R. Burleson, J. A. Faucett, R. L. Boudrie, W. B. Cottingame, S. J. Greene, C. L. Morris, Z. F. Wang, J. W. McDonald, C. Fred Moore, S. Mordechai, A. L. Williams, P. A. Seidlo, M. A. Bryan, S. Nanda, and S. J. Seestrom-Morris, Phys. Rev. C **35**, 1148 (1987).

[14] S. S. Kamalov, L. Tiator, and C. Bennhold, Phys. Rev. C **47**, 941 (1993).